Intracellular Clusterin inhibits mitochondrial apoptosis by suppressing p53-activating stress signals and stabilizing the cytosolic Ku70-Bax protein complex

Ioannis P. Trougakos, Magda Lourda, Marianna H. Antonelou, Dimitris Kletsas, Vassilis G. Gorgoulis, Issidora S. Papassideri, Yonglong Zou, Lukas H. Margaritis, David A. Boothman and Efstathios S. Gonos

SUPPLEMENTARY INFORMATION

Materials and Methods

Cell lines and culture conditions. Human osteosarcoma Sa OS cells (p53-null) were cultured as described previously (12). Saos-2-Tet-hp53 cells (40) were cultured in Tet System Approved FBS (BD Biosciences) and p53 was induced by using 1 μg/ml doxocycline (DOX) (BD Biosciences). U-2 OS cells sensitization to DXR (Adriamycin®; Sigma) was assayed following cell exposure to 1 μM of the drug for 24 h. Human ovarian SKOV-3 (p53-null), lung A549 (WT-p53) and breast MCF-7 (WT-p53) cancer cells were cultured in 5% FBS-containing DMEM.

Sequence and specific characteristics of the sCLU siRNA oligonucleotide. The sCLU siRNA oligonucleotide targets the 5'-GatgaagactctgctgctgttTG-3' region of the sCLU mRNA (Sense siRNA, 5'-ugaagacucugcugcuguuT_dT_d-3'; antisense siRNA, 5'-aacagcagcagagucuucaT_dT_d-3'), has no secondary structure stretches, a 47.4% GC content and is of the NA(N21) type; the 3' end of the sense siRNA was converted to TT. Analysis of its thermodynamic stability (MWG; http://www.mwgdna.com/html/all/index.php) revealed a high local free energy which indicates a very efficient silencing. The sCLU oligonucleotide fulfils 7 out of the 8 criteria previously set for efficient silencing (21), whereas the Cl-I oligonucleotide (12) fulfils five out of the eight criteria in the set.

$sCLU_I$ siRNA oligonucleotide synthesis, cell transfection and cell death measurement. The $sCLU_I$ siRNA oligonucleotide has been described previously (13). All apoptotic analyses in SKOV-3, A549 and MCF-7 cancer cell lines were performed by flow cytometry using concomitant TUNEL and $subG_1$-G_0 analyses. The p53 siRNA oligonucleotide used to suppress p53 expression in MCF-7 cells after sCLU knock down has been described previously (13).

siRNAs specificity and controls. All siRNA oligonucleotides used were extensively BLAST searched to verify either no homology to any other know human gene (Sc-I, Sc-II) or sCLU specificity (sCLU, $sCLU_I$, Cl-I). Applied controls for the verification of definitive loss-off-function data by the siRNAs

utilized were performed as described elsewhere [see, Editorial "Whither RNAi?". (2003). Nat. Cell Biol. 5, 489-490]. More specifically, cells were treated with siRNA-free transfection medium (mock) and scrambled siRNAs (specificity control, Figure 1; Supplementary Figures S1, S2 and S3). The effectiveness of sCLU gene silencing was analyzed at both the mRNA and protein levels (basic control, Figure 1A; Supplementary Figure S3). siRNA effects were titrated at 30, 10 and 1 nm exactly as described in "Materials and Methods" (quantitative control, Supplementary Figure S2B) and were verified by using siRNAs (Cl-I, $sCLU_I$, sCLU) that target distinct sites of the CLU mRNA (multiplicity control, Figure 1; Supplementary Figures S1, S2 and S3).

Immunoblotting analysis of cell culture supernatants, antibodies. Culture medium samples were prepared as described previously (22). Samples were adjusted by Bradford (BioRad), mixed with reducing Laemmli buffer and proteins were fractionated by SDS-PAGE followed by immunoblotting (22). Immunoblotting antibodies: α-tubulin (DM1A; Calbiochem), Band 3 (B-9277, Sigma), GRP78 (sc-1050; Santa Cruz biotech), Haemoglobin (Hb) (CR8000GAP, Europa Bioproducts).

Immunofluorescence staining and Confocal Laser Scanning Microscopy (CLSM). ER and Golgi were immunostained by using the SelectFX™ Alexa Fluor® 488 ER Labeling Kit (S34200, Invitrogen) and a mouse monoclonal antibody against human Golgin-97 (A-21270, Invitrogen) respectively.

Preparation of RBC membranes and cytosol. Venous blood from healthy volunteers was collected in EDTA-heparin containing tubes and RBCs were separated by low speed centrifugation (3,000 x g, 10 min). RBC membranes without Hb (white ghosts) were prepared by hypotonic lysis of RBCs in phosphate buffer (41) containing protease inhibitors. The ghosts were collected by high speed centrifugation (17,500 x g, 20 min) and washed thoroughly. The haemolysate collected after the first centrifugation of the ghost preparation was re-centrifuged to remove any contaminating membrane debris; the collected supernatant represents the RBC cytosol.

sCLU immunogold localization in RBCs and TEM. RBCs were fixed in 4% paraformaldehyde, 0.1% glutaraldehyde in PBS, pH 7.2 and embedded in Unicryl resin. Thin sections were probed with antibodies against Hb, Band 3 and sCLU (sc-5289, Santa Cruz). Detection of primary antibodies and samples examination was performed as described in "Materials and Methods".

References

40. Gorgoulis VG, Zacharatos P, Kotsinas A, et al. p53 activates ICAM-1 (CD54) expression in an NF-kappaB-independent manner. EMBO J 2003;22:1567-78.

41. Dodge JT, Mitchell C, Hanahan DJ. The preparation and chemical characteristics of hemoglobin-free ghosts of human erythrocytes. Arch Biochem Biophys 1963;100:119-30.

Figure legends

Figure S1. sCLU-depletion mediated effects in U-2 OS cells. (A) Schematic representation of relative sites in the CLU gene targeted by siRNA oligonucleotides used (Cl-I, sCLU and $sCLU_I$). (B) Immunoblot analyses of cell culture supernatants following cell transfection with shown siRNAs. A serum protein was used as reference for equal protein loading; molecular weight markers are shown to the right of the blot. (C) Analyses of cell morphology after sCLU-depletion (sCLU) showed significant cell shrinkage (arrows) and fewer cells per colony (dashed arrow) as compared to controls (Sc-I). Scale bars, 50 μm. (D) Direct cell counting of the adherent cells (n=3) following cell transfection with the indicated siRNAs. Assays shown were performed 72 h after siRNA cell transfection. Error bars indicate ± s.d.; asterisks significance at $P<0.05$.

Figure S2. (A) Quantitation of cell-death-related DNA fragments (n=2) in adherent U-2 OS cells (upper panel; on-going cell death) or in cell culture supernatants (lower panel; cumulative cell death) 48 to 96 h post-transfection with either Mock or indicated siRNA oligonucleotide preparations. (B) Titration of the sCLU knock down mediated effects in U-2 OS cells. (B_1) Apoptosis measurement (n=2) after cell transfection with 30, 10 and 1 nM (Sc-I, sCLU) or 30 and 1 nM (Cl-I) siRNA oligonucleotides. The apoptotic effects at 1 nM siRNA concentration were diminished for the Cl-I and were significantly reduced for the sCLU siRNA oligonucleotide. (B_2) Immunoblot analyses of whole cell lysates probed with antibodies against sCLU, p53 and p21; cells were treated with the indicated siRNA concentrations. (C) sCLU knock down in the MCF-7 human breast cancer cell line. (C_1) Immunoblotting of sCLU after cell transfection with mock preparations, control (Sc-II) or sCLU-specific ($sCLU_I$) siRNA oligonucleotides. (C_2) Apoptosis measurement after sCLU knock down revealed a significant ~2.8-fold increase in the endogenous cell death that could only partially suppressed by siRNA-mediated p53 knock down and was completely inhibited with a pan-caspase inhibitor. (D) Measurement of apoptosis after effective sCLU knock down (not shown) in A549 cells revealed a ~3-fold increase in the endogenous spontaneous cell death. Assays were performed 72 h after siRNA transfection. GAPDH and α-tubulin were used as protein loading controls in (B_2) and (C_1), respectively. Error bars indicate ± s.d. and asterisks significance at $P<0.05$.

Figure S3. sCLU-depletion induces cell death in p53-null cell lines. (A) sCLU immunoblotting (upper panel) and apoptosis quantification (lower panel) following effective sCLU knock down ($sCLU_I$ siRNA) in the human ovarian cancer cell line SKOV-3. (B-E) sCLU depletion mediated affects in the Sa OS human osteosarcoma cell line. (B_1) Quantitative PCR (n=3; upper panel) and immunoblotting (lower panel) of the sCLU transcript and protein expression levels, respectively after cell transfection with the indicated siRNA oligonucleotides. The Cl-I and sCLU siRNAs reduce both the sCLU mRNA (upper panel) and protein (lower panel) expression levels by ~2.5- to 5-fold, respectively. (B_2) Immunoblot analyses of control or sCLU knocked down whole cell lysates probed with antibodies against Bax and Bcl-2. (C_1) Measurement of cumulative cell death (n=3) in control and sCLU knocked

down cells showed a moderate increase of spontaneous cell death in sCLU knocked down cells. (C_2) Comparative FACS analysis (shown data are representative of two independent experiments) in Sc-I and sCLU siRNA treated cells. A ~1.5-fold increase of the subdiploid fraction (indicative of apoptosis) and a moderate decrease of the S phase cells were found in sCLU-depleted cells. (D) Combined reinforced expression of p53 and sCLU-depletion in tetracycline-inducible $p53^{WT}$ Sa OS cells significantly enhanced apoptosis. Parental cells, treated (Sa OS-DOX, Sa OS $p53^{tet}$-DOX) or not (Sa OS, Sa OS $p53^{tet}$) with DOX to activate the p53 transgene expression, were transfected with the Sc-I, Cl-I and sCLU oligonucleotides and endogenous cell death was assayed (upper panel; n=2). The effective sCLU knock down and the p53 transgene induction, were verified by immunoblotting (lower panel). Blots were also probed with antibodies against Bax and Bcl-2. (E, upper panel) Immunoblotting of cytochrome c in cytosolic and mitochondrial cellular fractions following cell transfection with indicated siRNAs (for fraction purity see Figure $S6A_1$). (E, lower panel) Caspase-8 and caspase-9 activity measurement (n=2) as described in Figure 3D. All assays were performed 72 h after siRNA transfection unless otherwise indicated. GAPDH probing was used as a protein loading reference in (B_2) and (D). Error bars indicate ± s.d; asterisks significance at $P<0.05$.

Figure S4. (A, B) sCLU-depletion in U-2 OS cells disrupts the structure of the ER and Golgi compartments. (A_1) CLSM (upper and lower panels) and TEM (middle panel) sCLU immunolocalization in control and sCLU knocked down cells. For CLSM immunofluorescence cells were co-stained with anti-sCLU, anti-PDI (ER-marker, red) and DAPI. The three captured images were merged to reveal co-distribution sites. Selected antigen co-localization sites and nuclei are indicated by arrows and arrowheads respectively in (A_1), upper panel; the disrupted ER foam-like structure is shown with a dashed arrow in (A_1) lower panel. (A_1, middle panel) TEM immunogold localization of sCLU in ER and secretory vesicles (sv). Scale bars, CLSM, 10 μm; TEM, 100 nm. (A_2) GRP78 immunoblotting in whole cell lysates from control and sCLU-depleted cells; GAPDH was used as a normalizer. (B) Cells were co-stained with anti-sCLU, anti-Golgin-97 (Golgi-marker, red) and DAPI. Sites of sCLU and Golgin-97 co-localization are indicated by arrows (upper panel); the disrupted Golgi in sCLU-depleted cells is marked by a dashed arrow (lower panel). Scale bars, 10 μm. Assays were performed 72 h post-siRNA transfection. (C) sCLU localization in the plasma membrane and cytosol of RBCs. (C_1) Immunoblotting of sCLU in isolated plasma membrane (10 μg) and cytosol (100 μg) RBCs preparations; fraction purity was verified by reprobing with the major transmembrane (Band 3) and cytosolic (Hb) protein markers. (C_2) TEM sCLU immunogold localization in human RBCs. Cells were immunostained with an anti-sCLU monoclonal antibody or with antibodies against Band 3 and Hb. PM, plasma membrane; CYT, cytosol. Scale bar, 100 nm.

Figure S5. sCLU knock-down in U-2 OS cells promotes p53 translocation to mitochondria. (A) Immunoblot analysis of p53 in isolated cytosolic (cyt) and mitochondrial (mt) fractions of control or sCLU knocked down cells (see also, Fig. 4A and 5A). (B) CLSM immunolocalization of p53 after

staining control or sCLU-depleted cells with anti-p53, mitotracker and DAPI. The captured images were merged to reveal antigen co-localization with mitochondria (dashed arrows, lower panel). Scale bars, 10 μm.

Figure S6. sCLU-depletion in Sa OS cells promotes mitochondrial accumulation of activated Bax due to disruption of the Ku70-Bax protein complex. (A_1) Immunoblot analyses of cytosolic and mitochondrial fractions following cell transfection with the indicated siRNA oligonucleotides. Blots were probed with antibodies against Bax and Ku70. Immunoblot quantitation (n=2) showed a ~4.5-fold increase in the amount of Bax that co-purified with mitochondria (A_1, second panel from top); fraction purity was verified by blot probing with anti-OxP-IV and anti-PCNA. (A_2) CLSM immunolocalization of Bax in control and sCLU-depleted cells. Cells were co-stained with an anti-Bax antibody, mitotracker and DAPI and the captured images were merged to reveal levels of Bax co-localization with mitochondria (dashed arrows, lower panel). Scale bars, 10 μm. (B_1-B_3) Quantitative immunoprecipitation analyses of the sCLU, Ku70 and Bax proteins interaction in control and sCLU-depleted cells. Transfected cells were lysed in CHAPS buffer and lysates were immunoprecipitated (IP) under reducing conditions *(R)* with antibodies against active Bax (B_1, antibody Bax^{6A7}), total Bax (B_2) and sCLU (B_3). Immunoprecipitates were probed (IB) with anti-Ku70, anti-sCLU and anti-Bax antibodies. Quantitative analyses of either Bax activation or Ku70-Bax dissociation (n=2) after sCLU-depletion are shown in (B_1) and (B_2) respectively (second panels from top). Equal protein input in the quantitative immunoprecipitations was demonstrated by GAPDH or Ku70 probing of unprocessed fractions. siRNA-related assays were performed 72 h post-transfection. Bars denote ± s.d.; asterisks significance at $P<0.05$.

Figure S7. sCLU-Ku70-Bax binding is disrupted during chemotherapeutic drug mediated mitochondrial apoptosis in U-2 OS cells. Exponentially growing U-2 OS cells (CON) or cells exposed to 1 μM DXR for 24 h (DXR) were fractionated in cytoplasmic and nuclear preparations and lysates were immunoprecipitated under reducing conditions in CHAPS lysis buffer with antibodies against sCLU, Ku70 and Bax. The immunoprecipitates were probed with antibodies against sCLU, Ku70, Ku80 and Bax. sCLU and Ku70 interact mainly in the cytoplasm of both normally growing and drug-treated cells. Quantitative analyses (shown at the graphs) of cytoplasmic Bax association with Ku70 or sCLU revealed reduced binding after cell exposure to DXR. The fact that Ku70 did not bind sCLU in yeast-two-hybrid analyses (4) indicate that Bax (or other factors) is (are) required for Ku70-sCLU interaction. Alternatively, in yeast-two-hybrid, either most Ku70 is tightly bound to Ku70-Ku80 complex or yeast does not provide sCLU with correct post-translational modifications for Ku70 binding. Equal protein input in the quantitative immunoprecipitations was demonstrated by Ku70 probing of unprocessed fractions.

Figure S8. sCLU-depletion-mediated mitochondrial relocation of Bax in Sa OS cells relates to the disruption of a cytoplasmic sCLU-Ku70-Bax nexus. (A) CLSM staining of Sc-I or sCLU siRNA transfected cells, with anti-Ku70 (goat polyclonal antibody, blue), anti-Bax (rabbit polyclonal antibody, green) and mitotracker. Captured images were merged to reveal co-localization sites. The cytosolic co-localization of Ku70 and Bax in Sc-I treated cells is denoted by arrowheads (upper panel); co-localized Bax and mitochondria in sCLU-depleted cells are indicated by dashed arrows (lower panel). Scale bars, 10 μm. (B) Triple staining of control or sCLU-depleted cells with anti-sCLU (goat polyclonal antibody, blue), anti-Ku70 (mouse monoclonal antibody, green) and anti-Bax (rabbit polyclonal antibody, red) antibodies. In control cells all three antigens co-localize mostly at the cytoplasm (white areas; upper panel, arrows). Following sCLU-depletion, Ku70 does not co-localize with Bax (dashed arrows, lower panel). Assays were performed 72 h post-siRNA-transfection. Scale bars, 10 μm. (C) CLSM-derived quantitative analysis of fluorochromes co-localization in Ku70-Bax-mitochondria (left graph) and sCLU-Ku70-Bax (right graph) triple staining preparations. Analyses were performed as described in Figure 6C by using Vol*ocity* software. Error bars denote ±s.d. and asterisks significance at $P<0.05$.

Figure S9. Schematic representations of the sCLU-depletion-mediated molecular effects in human cancer cells. Depletion of sCLU destructs the ER-Golgi compartments and promotes mitochondria aggregation. The released stress signals activate p53 (B) or other, currently unknown, factors in a p53-null (A) cellular context. Given that sCLU binds and stabilizes the cytoplasmic Ku70-Bax complex, its depletion releases Bax from Ku70 rendering Bax in an active state that translocates to mitochondria. This cascade of events along with down-regulation of other potent Bax inhibitors, namely Bcl-2 and Bcl-X_L, triggers cytochrome c release in the cytosol, caspase-9 activation and apoptosis. In a wild type p53 cellular context (B) activated p53 accumulates in both the mitochondria and nucleus. In the nucleus p53 triggers p21 and Bax (or other BH3-only pro-death) genes activation. The former arrests cells at the G_1-S checkpoint whereas the latter accumulates in the mitochondria triggering apoptosis. Thus, p53 essentially acts as an amplifier of the apoptotic outcome. The observed G_1-S arrest occurs independently of the Rb-$p16^{INK4a}$ regulatory axis since U-2 OS cells are $p16^{INK4a}$ null, whereas Sa OS cells, which do not arrest growth after sCLU-depletion, express wild-type $p16^{INK4a}$ (unpublished data).

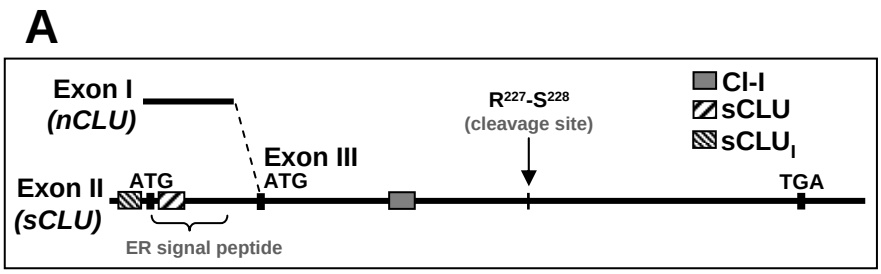

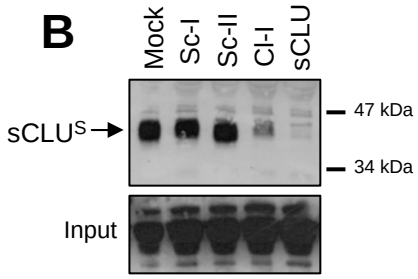

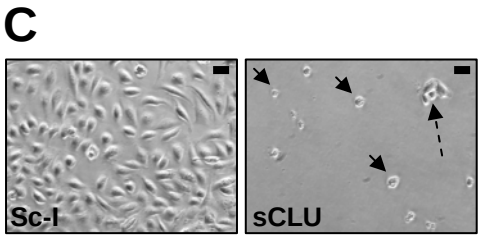

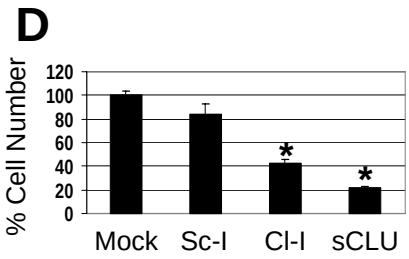

Trougakos et al / Suppl. Figure S1

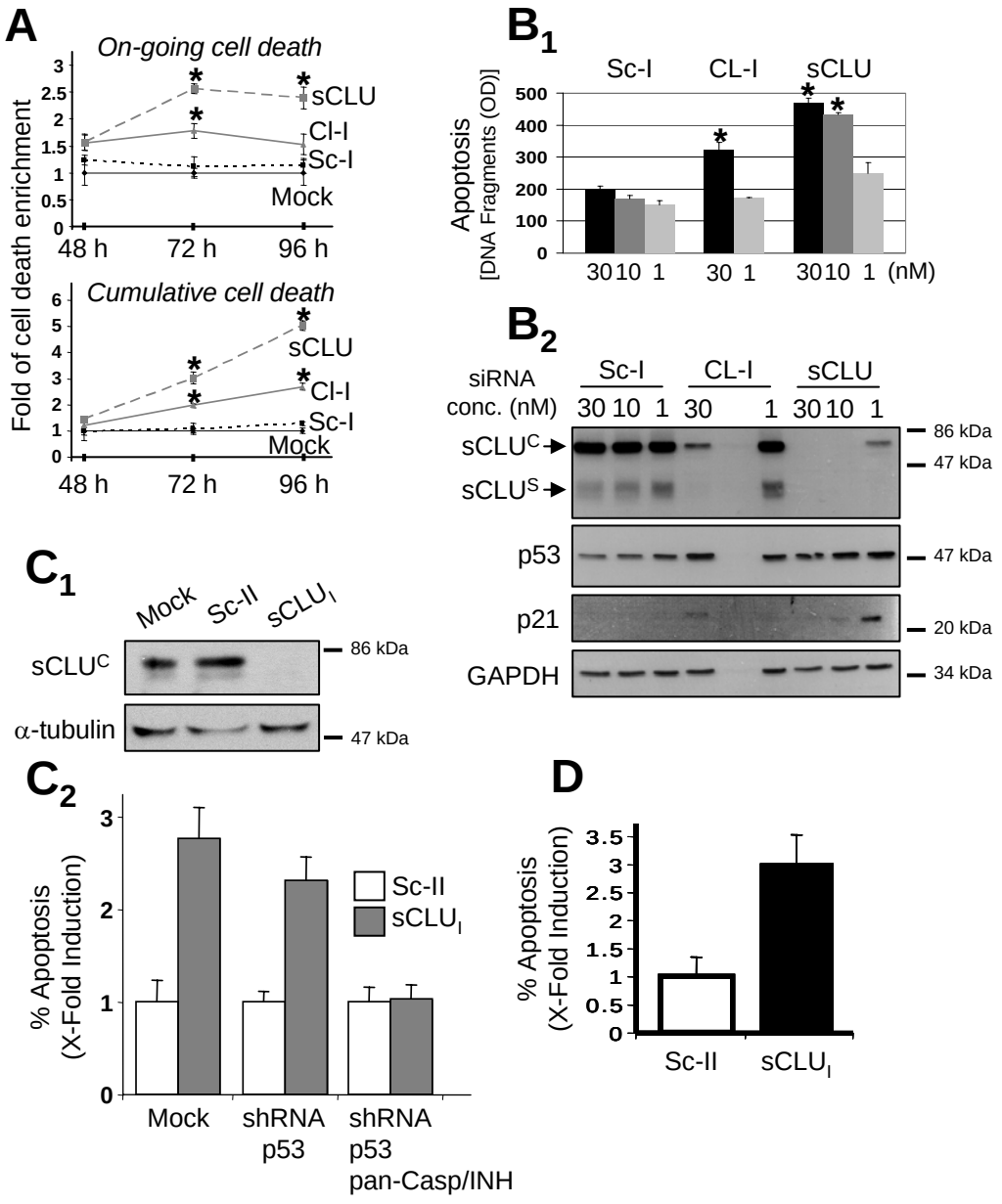

Trougakos et al / Suppl. Figure S2

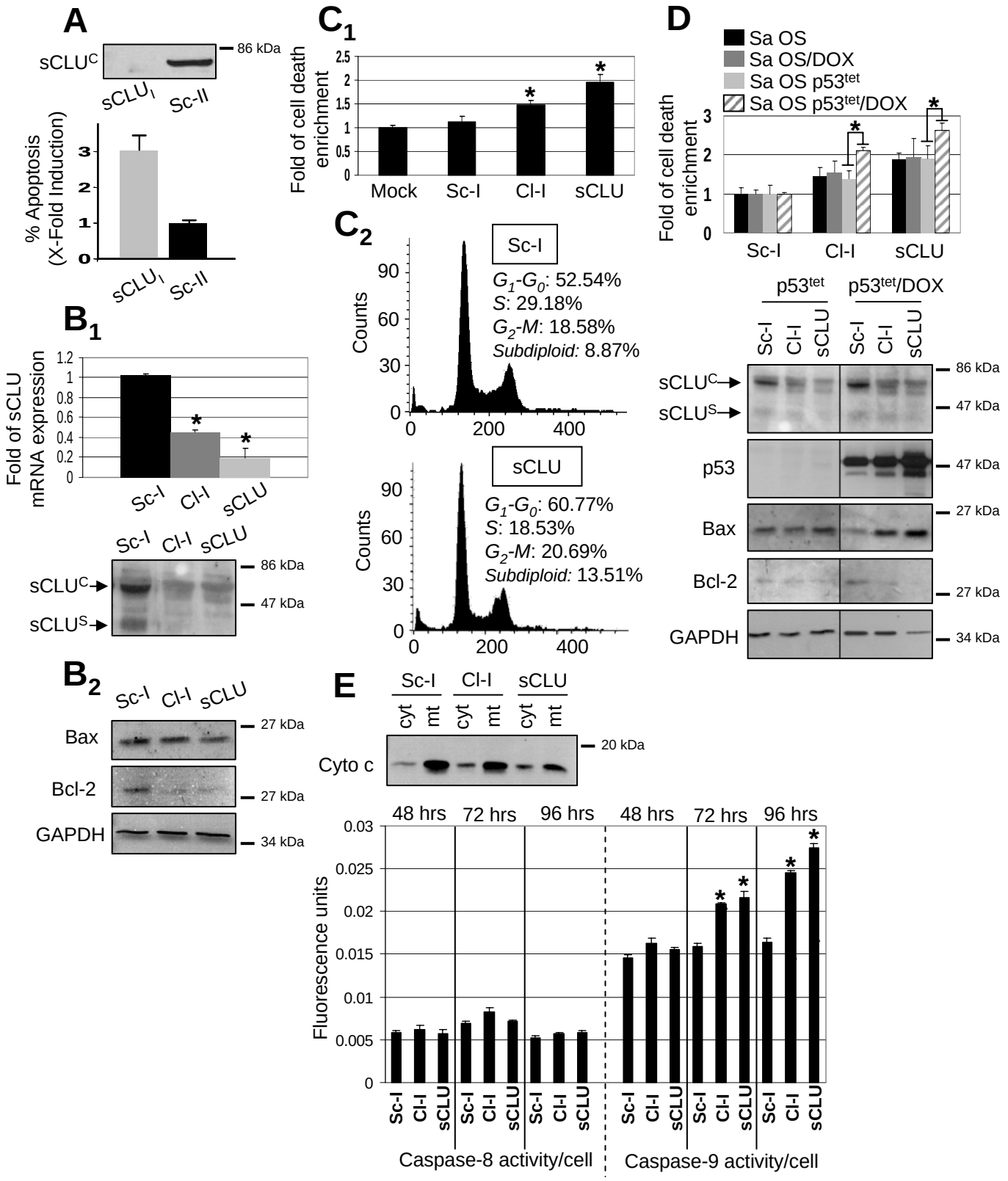

Trougakos et al / Suppl. Figure S3

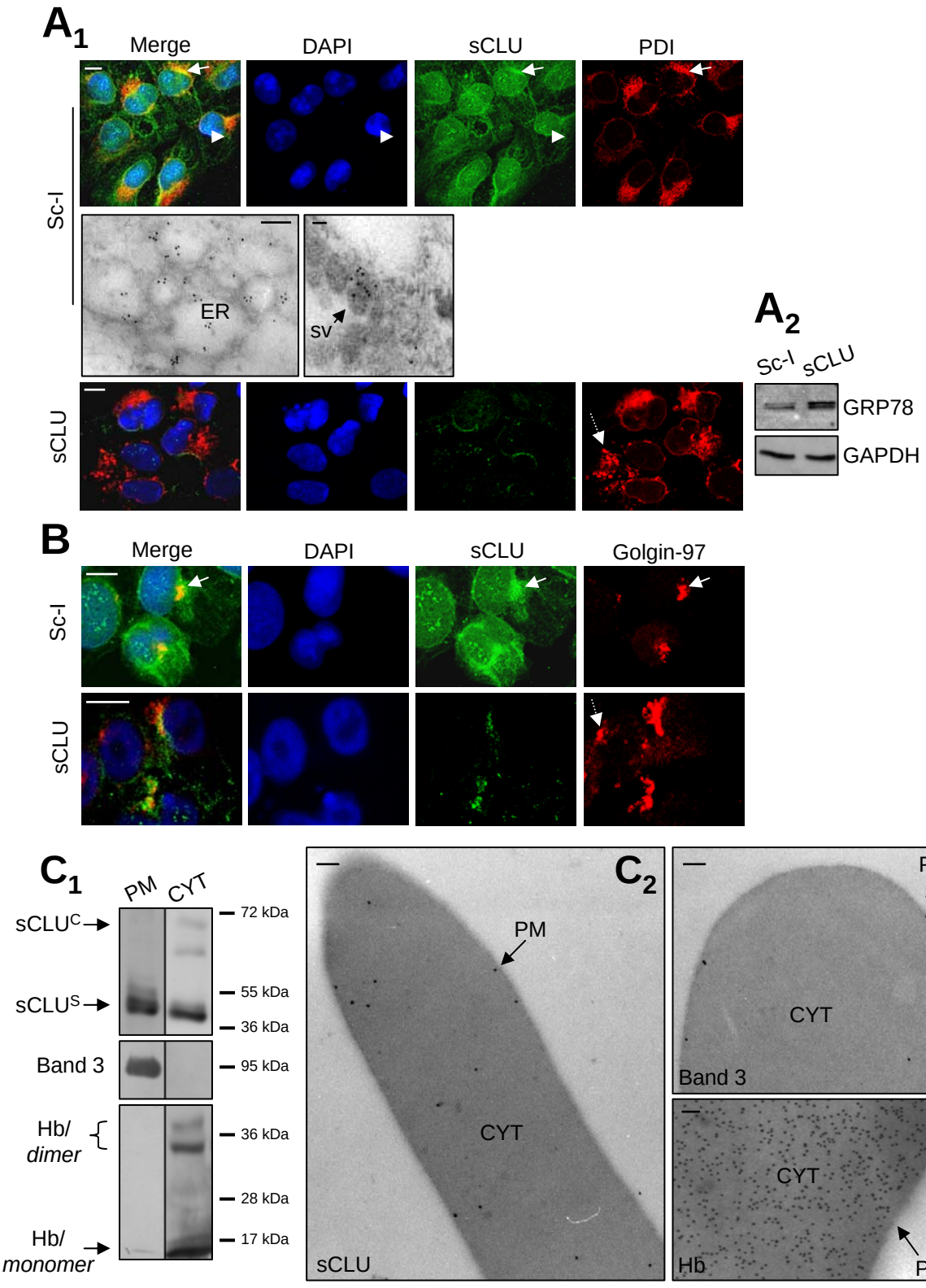

Trougakos et al / Suppl. Figure S4

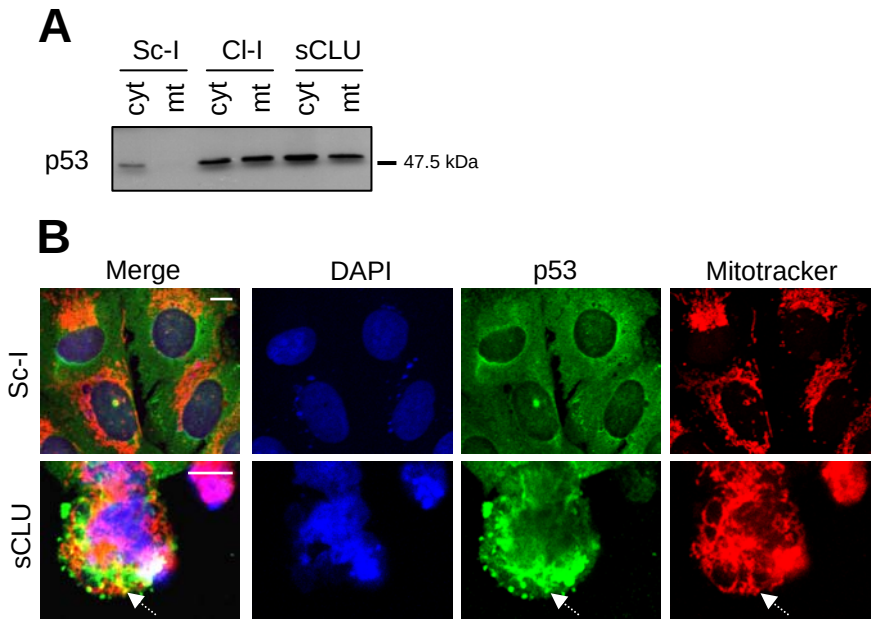

Trougakos et al / Suppl. Figure S5

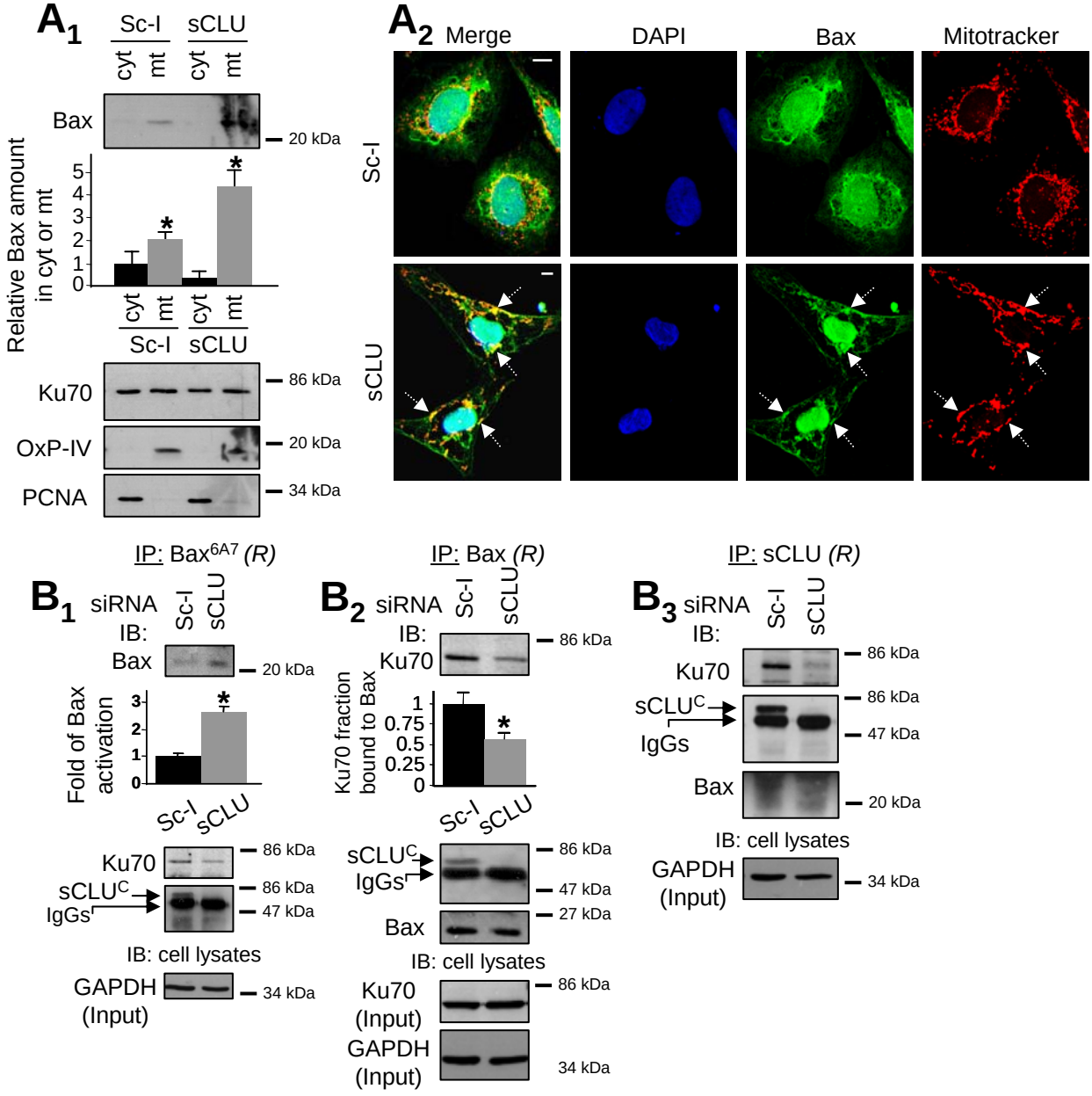

Trougakos et al / Suppl. Figure S6

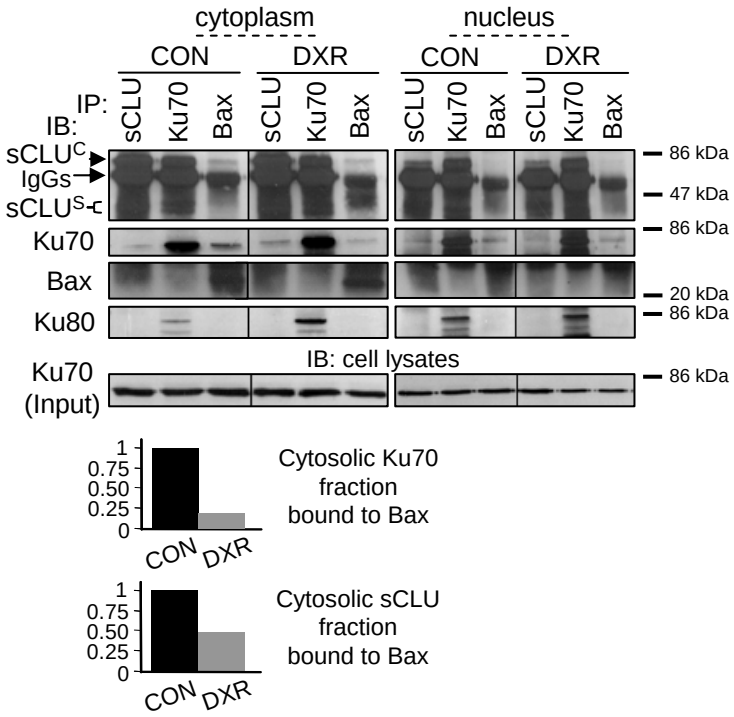

Trougakos et al / Suppl. Figure S7

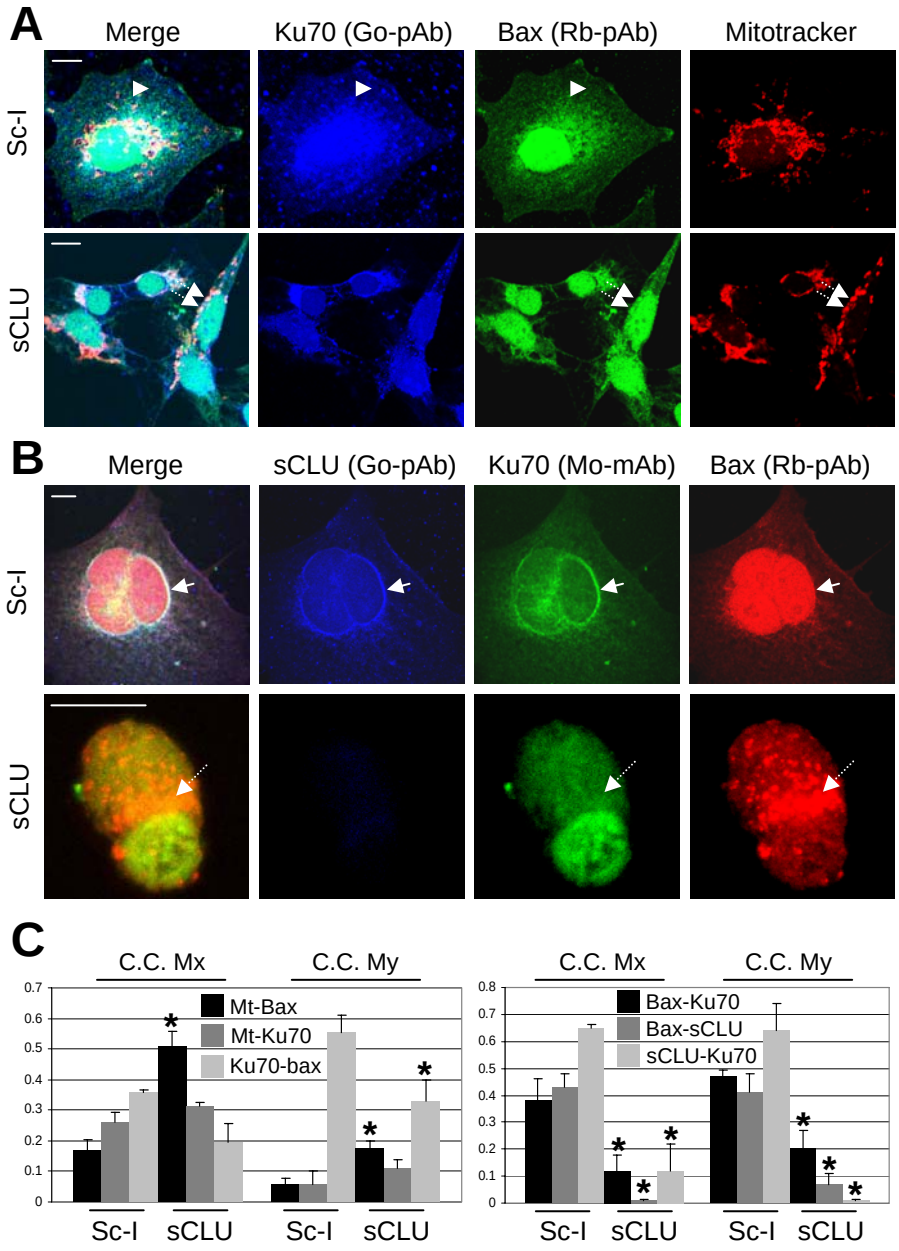

Trougakos et al / Suppl. Figure S8

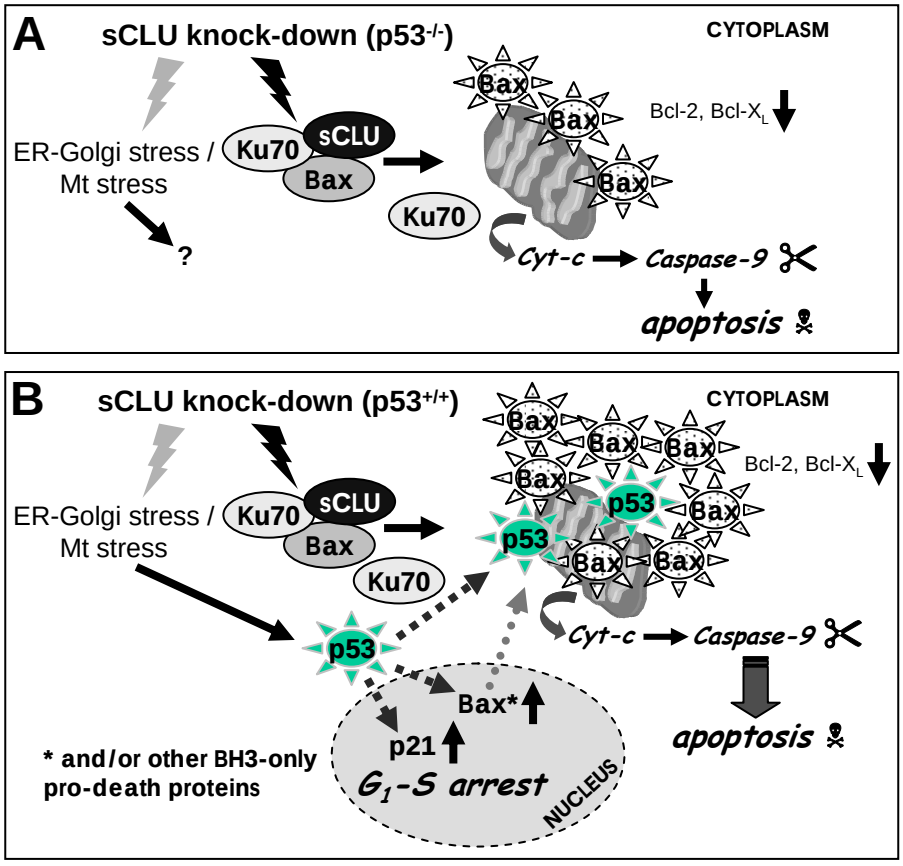

Trougakos et al / Suppl. Figure S9